Inhibition of DNA-PK with AZD7648 Sensitizes Tumor Cells to Radiotherapy and Induces Type I IFN-Dependent Durable Tumor Control

Kyoko Nakamura[1], Ankur Karmokar[1], Paul M. Farrington[1], Neil H. James[1], Antonio Ramos-Montoya[2], Susan J. Bickerton[1], Gareth D. Hughes[2], Timothy M. Illidge[3], Elaine B. Cadogan[2], Barry R. Davies[2], Simon J. Dovedi[2], and Viia Valge-Archer[2]

ABSTRACT

Purpose: Combining radiotherapy (RT) with DNA damage response inhibitors may lead to increased tumor cell death through radiosensitization. DNA-dependent protein kinase (DNA-PK) plays an important role in DNA double-strand break repair via the nonhomologous end joining (NHEJ) pathway. We hypothesized that in addition to a radiosensitizing effect from the combination of RT with AZD7648, a potent and specific inhibitor of DNA-PK, combination therapy may also lead to modulation of an anticancer immune response.

Experimental Design: AZD7648 and RT efficacy, as monotherapy and in combination, was investigated in fully immunocompetent mice in MC38, CT26, and B16-F10 models. Immunologic consequences were analyzed by gene expression and flow-cytometric analysis.

Results: AZD7648, when delivered in combination with RT, induced complete tumor regressions in a significant proportion of mice. The antitumor efficacy was dependent on the presence of $CD8^+$ T cells but independent of NK cells. Analysis of the tumor microenvironment revealed a reduction in T-cell PD-1 expression, increased NK-cell granzyme B expression, and elevated type I IFN signaling in mice treated with the combination when compared with RT treatment alone. Blocking of the type I IFN receptor *in vivo* also demonstrated a critical role for type I IFN in tumor growth control following combined therapy. Finally, this combination was able to generate tumor antigen-specific immunologic memory capable of suppressing tumor growth following rechallenge.

Conclusions: Blocking the NHEJ DNA repair pathway with AZD7648 in combination with RT leads to durable immune-mediated tumor control.

Introduction

Radiotherapy (RT) is an important part of the standard of care and is used in the treatment of 50% to 60% of all patients with cancer (1). RT induces single- and double-strand DNA breaks leading to cell death by mitotic catastrophe and apoptosis (2). Therefore, RT also leads to the activation of multiple DNA damage response (DDR) pathways that can repair this damage, and can contribute to intrinsic tumor cell radio-resistance (3). For that reason, combinations of RT with DDR inhibitors are potentially attractive therapeutic opportunities to improve tumor control. Inhibition of early DDR signaling mediators, including ataxia telangiectasia and Rad3-related (ATR; refs. 4–6), poly (ADP-ribose) polymerase (PARP; refs. 7–9), ataxia telangiectasia mutated (ATM; refs. 10–13), or DNA-dependent protein kinase (DNA-PK; refs. 14–17), which are activated in response to replication stress, single-strand breaks, and DSB, has been shown to potentiate both RT and chemotherapy.

Emerging evidence suggests that the antitumor activity of RT may extend beyond direct DNA damage effects in the tumor to the activation of antitumor immune responses (18–21). Preclinical studies demonstrate that the release of proinflammatory cytokines such as type I IFN and expression and/or release of damage associate molecular patterns (DAMP) including High Mobility Group Box 1 (HMGB1) and adenosine triphosphate (ATP) following cytoreductive therapy promote dendritic cell (DC) activation and priming of tumor-associated antigen (TAA)-specific T cells (22, 23). Furthermore, fragmented genomic or mitochondrial DNA following RT or chemotherapy can be recognized by pattern-recognition receptors (PRR) such as TLR9 or cyclic GMP-AMP synthase (cGAS)-stimulator of interferon genes (STING), which stimulate the expression of pro-inflammatory cytokines including type I IFN (24–27). In turn, type I IFN increases the expression of costimulatory molecules including CD40, CD80/86, and MHC class II on DC enhancing their T-cell priming capacity (24, 25, 28, 29). Despite this, RT alone rarely leads to a curative response, suggesting that competent systemic antitumor immune responses are rarely engendered. Strategies to augment the immunogenicity of RT are urgently needed.

DNA-PK is a nuclear serine/threonine kinase, which is activated in the early phase of nonhomologous end joining (NHEJ) in the DNA DSB repair pathway. DNA-PK also plays an important role in V(D)J recombination and immuno-globulin class switch recombination by joining the DNA ends generated by RAG endonuclease during T-cell and B-cell development (30, 31). We and other groups have previously reported that DNA-PK inhibition is an effective radiosensitizer and can induce sustained tumor regression in human tumor xenografts

[1]Bioscience, Early Oncology, Oncology R&D, AstraZeneca, Alderley Park, Macclesfield, United Kingdom. [2]Bioscience, Early Oncology, Oncology R&D, AstraZeneca, Cambridge, United Kingdom. [3]Targeted Therapy Group, Division of Cancer Sciences, University of Manchester, Christie Hospital, Manchester NIHR Biomedical Research Centre, Manchester, United Kingdom.

Note: Supplementary data for this article are available at Clinical Cancer Research Online (http://clincancerres.aacrjournals.org/).

S.J. Dovedi and V. Valge-Archer contributed equally to this article.

Corresponding Author: Simon J. Dovedi, Oncology R&D, AstraZeneca, Cambridge CB21 6GH, UK. E-mail: simon.dovedi@astrazeneca.com

Clin Cancer Res 2021;27:4353–66

doi: 10.1158/1078-0432.CCR-20-3701

Translational Relevance

Inhibiting the DNA damage response mechanism is a promising strategy for enhancing the efficacy of chemotherapy and radiotherapy in cancer treatment. DNA-dependent protein kinase (DNA-PK) is a key mediator of nonhomologous end joining, and is involved in repairing double-strand breaks. It has been shown that AZD7648 is a potent and selective DNA-PK inhibitor and has radiosensitizing effects. Here, we show that AZD7648 with radiotherapy not only increases cancer cell death via increased DNA damage, but also that cell death is immunogenic, inducing $CD8^+$ cytotoxic T cells and type I IFN–dependent antitumor responses. As the result, significant tumor growth control was observed in preclinical models.

Our research highlights the important role of tumor microenvironment and immunologic memory in the mechanism of this combination, suggesting that efficacy may be greater than predicted by immunodeficient models. Phase I/II clinical trials for AZD7648 in combination with chemotherapy (NCT03907969) and radiotherapy (NCT04550104) are ongoing.

and patient-derived xenograft (PDX) models when administered concurrently with RT or chemotherapy (14–17, 32). However, to date, no study has investigated the immunologic consequences of this combination, which limits the translational understanding of the clinical potential for this approach. In this study, we use fully immunocompetent tumor-bearing mice to integrate our understanding of the tumor intrinsic radiosensitization and immunologic consequences of combination therapy with the DNA-PK inhibitor AZD7648 and RT. Our data demonstrate that in addition to direct tumor cell radiosensitization, the combination of AZD7648 and RT leads to long-term durable responses which are type I IFN and $CD8^+$ T-cell dependent.

Materials and Methods

Cell lines

CT26 and B16-F10 cells were purchased from ATCC. MC38 cells were from NCI. All cells were stored and quality checked at in-house cell bank facility. Cells were confirmed to be negative for *Mycoplasma* contamination by PCR test. Cells were authenticated by short tandem repeat analysis before creation of stock vials. Cells were cultured for fewer than 10 passages after resuscitation. MC38 cells were cultured with DMEM (Gibco, #41966)/10% FCS (Gibco, #10270)/2 mmol/L L-glutamine (Gibco)/1 mmol/L sodium pyruvate (Gibco)/1x MEM nonessential amino acid (Gibco, #11140) in 37°C, 7.5% CO_2 incubator. CT26 cells were cultured with RPMI1640 (Gibco, #31870)/10% FCS/2 mmol/L L-glutamine in 37°C, 7.5% CO_2 incubator. B16-F10 cells were cultured with MEM (Gibco, #21090)/10% FCS/2 mmol/L L-glutamine/1 mmol/L sodium pyruvate/1x MEM nonessential amino acid in 37°C, 7.5% CO_2 incubator. For clonogenic cell survival assays, GlutaMAX Supplement (Gibco) was used in place of L-glutamine.

In vivo procedures

Female 5- to 12-week-old C57BL/6 (Charles River), Balb/c, and nude mice (Envigo) were used in this study. Three to five mice were housed in one cage. 1×10^7 MC38, 5×10^5 CT26, or 1×10^5 B16-F10 cells were subcutaneously implanted to the left flank. For the MC38 model, cells were implanted to mice in randomly assigned cage order and all tumor-bearing animals were used for studies. Dosing started at day 3 to 4 post-implant when the tumor volume reached 0.1 to 0.2 cm^3. For CT26 and B16-F10 models, mice were randomized by tumor size at 7 to 9 days after implant when the tumor volume reached 0.1 to 0.2 cm^3 using in-house randomization tool. AZD7648 (75 mg/kg) was resuspended with 0.5% hydroxypropyl methylcellulose + 0.1% Tween-80 and orally dosed 1 to 2 hours before the tumor-targeted X-ray irradiation (IR). Mice were anaesthetized with Ketamine (37.5, 30, and 26 mg/kg for Nude, Balb/c, and C57BL/6 respectively, for the first 3 days, reducing to 33.75, 27, and 23.4 mg/kg for Nude, Balb/c, and C57BL/6 respectively, for the 2 remaining days of the RT treatment cycle) and Medetomidine cocktail (0.5 mg/kg) by subcutaneous injection. Anaesthetized mice were placed laterally on lead plate shielding with apertures (1 cm diameter for small and 1.5 cm for large tumors) to ensure the entire tumor was exposed to the IR field. RT was delivered using a 320 X-ray (Gulmay Medical Inc.) at dose rate of 0.235Gy/mA/min (2Gy by 320 V, 5 mA, 1.7 minutes, 6Gy by 320 V, 8 mA, 3.2 minutes, 7Gy by 320 V, 8 mA, 3.7 minutes). Mice received at least 20 minutes of induction with anesthetic, and posttreatment received the reversal agent, atipamezole (0.5 mg/kg), and 300 μL of warm saline administrated subcutaneously. Oxygen was supplied to chambers incubated at 26 to 28°C during both the anesthetic induction and recovery periods.

For the tumor rechallenge experiments, cells were implanted contralaterally with respect to the initial tumor implantation into mice with completely regressed primary tumors. Naïve control mice were also implanted at the same time, as growth controls.

For the depletion and blocking studies, mice were treated with anti-CD8α (YTS169.4), anti-CD4 (GK1.5), anti-NK1.1 (PK136) and anti-IFNαR1 (MAR1–5A3; BioXcell). Specifically, anti-CD8α antibody (10 mg/kg) was administered on days 2, 3, 10, 11, and 18; 12.5 mg/kg of anti-CD4 antibody was administered on days 3 and 4 then reduced to 5 mg/kg on days 13, 20, and 27; anti-NK1.1 antibody (10 mg/kg) was administered on days 2, 3, 11, and 25; and anti-IFNαR1 antibody (5 mg/kg) was administered three times per week for 5 weeks starting on day 2 via intraperitoneal injection.

All animal procedures were conducted according to UK Home Office guidelines (Home Office project licenses 70/8839, 70/8893, 70/8894, and PP3208003), the Animal Scientific Procedures Act 1986, and protocols were approved by a local animal welfare and ethical review body.

Tumor growth rate

Tumor growth rate was calculated using an in-house program based on fitting each tumor's growth curve to an exponential model [$\log_{10}(\text{tumor volume}) = \alpha + \beta \times \text{time} + \text{error}$; α and β are parameters that correspond to the log initial volume and growth rate, respectively].

Western blotting

Tumor and cell line lysates were prepared using KDR lysis buffer (20 mmol/L Tris pH 7.5, 127 mmol/L NaCl, 10% glycerol, 50 mmol/L NaF, 1 mmol/L Na_3VO_4) with protease complete inhibitor tablet (Roche), phosphatase inhibitor cocktail 2 and 3 (Sigma), protease inhibitor cocktail (Sigma), Benzonase nuclease (Sigma), 1% SDS, and 1% NP40. Tumors were homogenized in lysis buffer in Fast Prep 2 mL tube with matrix A (MP biomedicals) using a Fast Prep-24 5G instrument (MP biomedicals). Protein concentration was determined using BCA Protein Assay Kit (Pierce). Twenty-five to 53 μg of protein

was separated by NuPAGE BisTris gel 4% to 12% and transferred to nitrocellulose membrane using Iblot2 dry blotting systems (Thermo Fisher Scientific). Membranes were blocked with 5% skim milk in TBS-0.05% Tween20 solution.

The following antibodies were used for protein detection: anti-phospho H2AX Ser139 (Cell Signaling Technology, #2577), anti-phospho RPA32 S4/S8 (Bethyl Laboratories, #A300-245A), anti-phospho Chk-1 Ser345 (Thermo Fisher Scientific, clone S.48.4), anti-β-actin (Cell Signaling Technology, clone 13E5), and anti-rabbit IgG-horseradish peroxidase conjugate (Cell Signaling Technology, #7074). Images were captured using a Syngene G box following addition of Super Signal West Dura or Femto extended duration substrate (Thermo Fisher Scientific). Signal intensity was analyzed using GeneTools software (Syngene).

Clonogenic cell survival assay

MC38 cells were plated at varying densities (200, 400, 800, 3,200, 12,800 cells/well) in a six-well plate in 3 mL culture medium and cultured overnight. AZD7648 stock solution (10 mmol/L) was made with DMSO, stored at −20°C, and diluted to final concentration with culture media on the treatment day. AZD7648 or DMSO control was added approximately 1 hour prior to treatment with 0, 2, 4, 6, or 8Gy IR. Cells were irradiated using Cabinet Irradiator CIX3 (Xstrahl) at dose rate of 2.02Gy/min (300 V, 10 mA) hardened by 0.7 mm Cu filter. Twenty-four hours later, the media was replaced (without compound) and culture continued for 7 to 8 days. Cell colonies were fixed and stained with Brilliant Blue G staining solution (Sigma) for 10 minutes after gentle washing with PBS. Excess staining solution was removed, washed with water, and images captured by GelCount colony counter (Oxford Optronix). Colony numbers were counted manually. Dose enhancing factor at 37% survival (DEF_{37}) was calculated as described previously (14).

Cell death analysis by flow cytometry

A total of 100,000 cells were plated in six-well plates in 3 mL culture medium and cultured overnight. AZD7648 or DMSO as control was added approximately 1 hour prior to IR. For caspase inhibition, 20,000 cells were plated in 24-well plates in 1 mL culture medium and next day, AZD7648 or DMSO with 20 μmol/L quinolyl-valy-O-methylaspartyl-[2,6-difluorophenoxy]-methyl ketone (QVD; Merck) was added 1 hour prior to IR. As a positive apoptosis inducing control, cells were treated with 10 nmol/L Staurosporine (Abcam). Cells were harvested with Trypsin-EDTA (Sigma) and resuspended with Annexin V binding buffer (Biolegend) 24, 48, and 72 hours after IR. A total of 1×10^5 cells were stained with Annexin-V APC or PE and Helix green as per manufacturer's protocol (Biolegend). Samples were analyzed using a FACS Canto (BD Bioscience) equipped with two lasers (488 and 640 nm) within 1 hour after staining and analyzed using FlowJo Software 10.6.1. (BD Bioscience).

Flowcytometry analysis of tumor-infiltrating leukocytes (TIL)

Freshly isolated tumor samples were processed using the Mouse Tumor Dissociation Kit (Myltenyi Biotec). Single cell suspensions were obtained by filtering through a 70 μm cell strainer. For flow cytometry, cell pellets were suspended in PBS (0.7 mL per 0.2 cm^3 tumor). Cells were stained with a Fixable Aqua Dead Cell Staining Kit (Thermo Fisher Scientific). Cells were incubated with anti-mouse CD16/32 antibody for Fc block (clone 93; Thermo Fisher Scientific). For intracellular/nuclear staining, cells were first stained for surface antigens then fixed/permeabilized with Foxp3/Transcription Factor Staining Buffer set (Thermo Fisher Scientific). Antibodies for flow cytometry included: CD45 (BD Bioscience or Thermo Fisher Scientific, clone 30-F11), CD8α (Biolegend, clone 53–6–7 or Thermo Fisher scientific, clone K15), CD3ε (BD Bioscience, clone 17A2), NKp46 (Biolegend, clone 29A14), GzmB (Thermo Fisher Scientific, clone GB12), CD19 (BD Bioscience, clone ID3), CD11b (BD Bioscience, clone M1/70), PD-1 (Biolegend 29F.1.A12 or Thermo Fisher Scientific, clone J43), Lag-3 (Thermo Fisher Scientific, clone eBioC9B7W), MHC class I tetramer consisting of murine H-$2K^b$ complex to KPSWETTL (MuLV p15e) peptide (MBL), and MHC class I tetramer consisting of murine H-$2K^b$ complex to SIINFEKL (OVA) peptide (MBL). Flow cytometry data were acquired using LSR Fortessa (BD Biosciences) equipped with five lasers (355, 405, 488, 561, and 640 nm) and analyzed with FlowJo Software 10.6.1. (BD Bioscience).

RNA extraction and qPCR

Tumor samples were harvested from mice, snap frozen in liquid nitrogen, and stored at −80°C. For RNA extraction, tumor samples were homogenized using TissueLyser systems with 5 mm stainless steel beads and RNA purified using an RNeasy Mini Kit (Qiagen). Cell lysates from *in vitro* cultures were prepared by adding RNA lysing buffer directly to the wells and RNA extracted using the RNeasy Mini Kit. RNA concentration was measured using NanoDrop spectrophotometers (Thermo Fisher Scientific).

For Fluidigm high throughput qPCR, 50 ng of RNA was reverse transcribed using the High-Capacity cDNA Reverse Transcription Kit (Applied Biosystems). cDNA was preamplified with TaqMan PreAmp Master Mix (Applied Biosystems). qPCR was performed in 96.96 dynamic array IFC (Fluidigm) with Gene Expression Master mix (Applied Biosystems) and FAM labelled TaqMan primer/probe master mix. Data were acquired in Biomark (Fluidigm). Each gene expression level was normalized to the average Ct values of three housekeeping genes, *Hprt, Ipo8*, and *Ywhaz*.

For 384-well plate-based qPCR, gene expression was measured using one step QuantiTect Probe RT-PCR Kit (Qiagen) with TaqMan probe/primer maser mix (Thermo Fisher Scientific) from 20 to 160 ng of RNA in a total assay volume 10 μL. Signal was detected using a Light Cycler 480 II (Roche). Gene expression levels were normalized to HPRT.

TaqMan probes used in this study are as follows: *Hprt* (Mm01545399_m1 for Light Cycler acquisition, Mm_03024075_m1 for Biomark acquisition), Ipo8 (Mm_01255158_m1), *Ywhaz* (Mm_01158416_g1), *Ddx4* (Mm_00802445_m1), *Ifit1* (Mm_00515153_m1), *Ifit2* (Mm_00492606_m1), *Ifit3* (Mm_01704846_s1), *Irf7* (Mm_00516793_g1), *Isg20* (Mm00469585_m1), *Mx1* (Mm_00487796_m1), *Mx2* (Mm_00488995_m1), *Rsad2* (Mm_00491265_m1), *Tnfsf10* (Mm_01283606_m1), *Ifnb1* (Mm_00439552_s1), *Cxcl10* (Mm_00445235_m1), and *Isg15* (Mm_01705338_s1; all from Thermo Fisher Scientific, FAM-MGB conjugate).

Statistical analysis

Statistical analysis was performed by GraphPad Prism v.8.0.2. (GraphPad), except for the *ex vivo* TILs FACS data. TILs FACS data statistics were analyzed using an AstraZeneca in-house program. Mean fluorescent intensity (MFI) is processed with a linear regression model treating treatment as a fixed effect where the variance is allowed to vary by treatment group. This analysis is equivalent to an unequal variance one-way ANOVA. The frequency data is processed with a beta regression, treating treatment as a fixed effect. *Post hoc* testing with no correction for multiple

testing is used to compare each treatment group to the reference group.

Results

AZD7648 inhibited the phosphorylation of its targeted proteins following irradiation in MC38 cells and tumor

To evaluate the inhibition of DNA-PK activity by AZD7648, phosphorylation of DNA-PK target proteins following IR in the MC38 murine tumor cell line was analyzed by Western blotting. We have previously showed that AZD7648 inhibits DNA-PK autophosphorylation at Ser2056 following IR by 50% at 91 nmol/L and approximately 90% at 1 μmol/L in A549 cells (14). At 30 minutes after 7Gy IR, H2AX^{Ser139}, RPA$^{Ser4/8}$, and Chk1^{Ser345} were highly phosphorylated. Treatment with 1 μmol/L AZD7648 prior to IR treatment inhibited target gene phosphorylation by approximately 40% after IR (**Fig. 1A** and **B**).

We next confirmed the impact of AZD7648 on the *in vivo* phosphorylation of DNA-PK target molecules in IR-treated tumors. MC38 tumor lysates were prepared and analyzed following the oral administration of AZD7648 (75 mg/kg) prior to a single dose of local 6Gy RT (**Fig. 1C**). When AZD7648 was administered 1 hour prior to RT, we observed a significant reduction in the phosphorylation of H2AX^{Ser139} and Chk1^{Ser345} ($P = 0.03$ and 0.01, respectively vs. RT only) to the baseline level seen in vehicle-only treated mice. AZD7648 pretreatment also resulted in a trend in reduction of RPA$^{S4/8}$ phosphorylation (AZD7648+RT vs. RT: 1.51 ± 0.38 vs. 2.31 ± 0.67, $P = 0.22$; **Fig. 1D–F**). In summary, AZD7648 inhibits the phosphorylation of DNA-PK target proteins following RT in MC38 cells both *in vitro* and *in vivo*.

DNA-PK inhibition by AZD7648 functions as a radiosensitizer

To test if AZD7648 enhances IR-induced MC38 cell death *in vitro*, apoptotic and necrotic cells were analyzed by flow cytometric detection of Annexin-V and DNA (Helix green). AZD7648 treatment without IR did not significantly change the percentages of Annexin-V$^+$Helix green$^-$ and Annexin-V$^+$Helix green$^+$ populations. A 7Gy dose of IR increased both populations at 24, 48, and 72 hours after IR whereas a lower dose (2Gy) increased those populations only slightly, which was statistically not significant. Pretreatment of cells with 1 μmol/L AZD7648 plus either dose of IR increased the percentage of the Annexin-V$^+$Helix green$^-$ population at all three time points whereas increases in the Annexin-V$^+$Helix green$^+$ population was observed only at the 48- and 72-hour time points. Treatment of cells with 100 nmol/L AZD7648 plus low-dose IR showed only modest

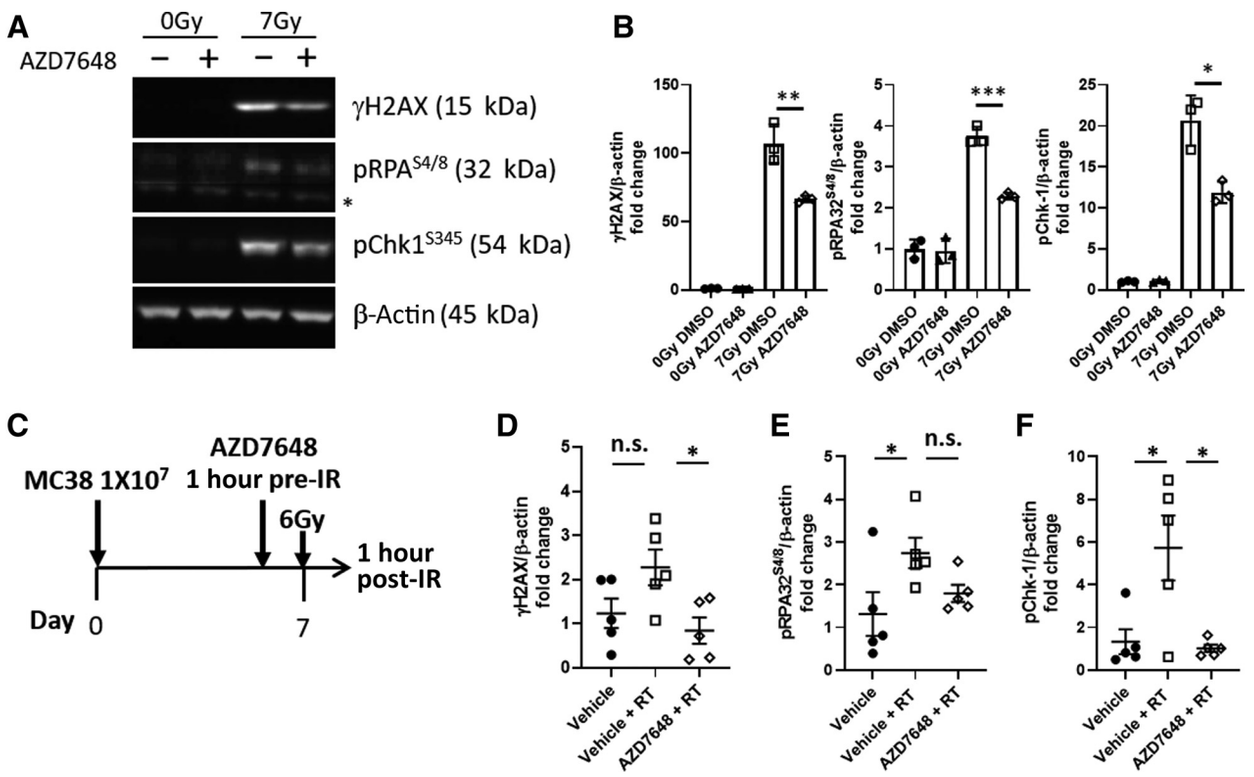

Figure 1.

AZD7648 inhibits the phosphorylation of DNA-PK substrates after IR. **A,** Western blot analysis of DNA-PK target protein phosphorylation in lysate from MC38 cells treated with AZD7648 1 μmol/L and 7Gy IR. Cell lysate was prepared 30 minutes after IR. * indicates nonspecific band. **B,** Fold change of phosphorylated target protein signal intensity level normalized by β-actin signal level from 0Gy DMSO control after 30 minutes after IR analyzed by Western blot analysis. $n = 3$, error bars represent mean and SD. Experiment was repeated three times and representative result was shown in figure. Unpaired *t* test, $^*P < 0.05$, $^{**}P < 0.01$, $^{***}P < 0.001$. **C,** Dosing schedule to MC38 bearing C57BL/6 mice. AZD7648 (75 mg/kg) was orally administrated 1 hour before tumor-targeted RT (6Gy) and tumor was harvested 1 hour after RT. **D–F,** Fold change of phosphorylated target protein signal intensity levels normalized by β-actin protein signal levels from vehicle control. Each dot represents a value from each animal. $n = 5$, error bars represent mean and SE, one-way ANOVA, Tukey's multiple comparison test (*, $P < 0.05$; n.s., nonsignificant).

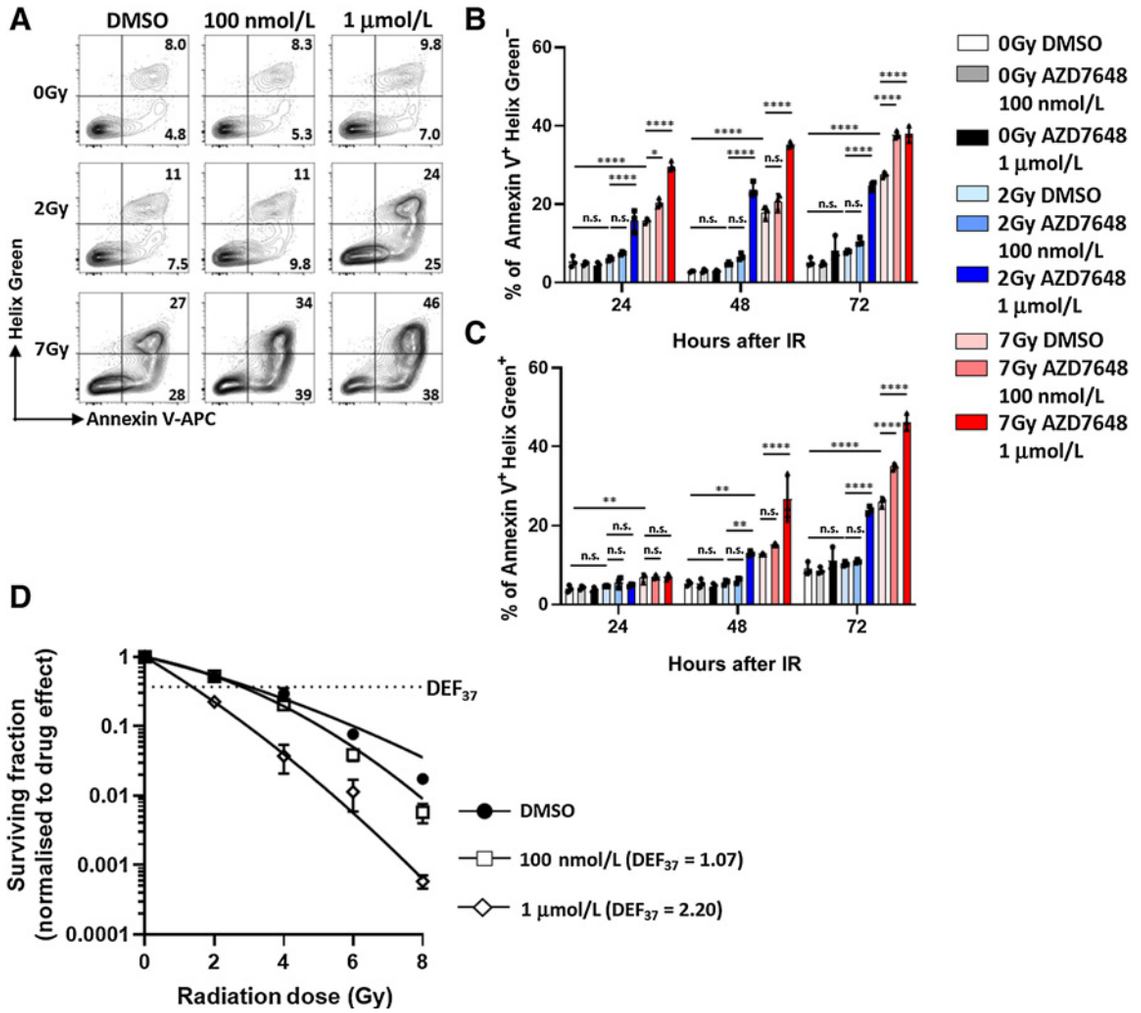

Figure 2.

AZD7648 radiosensitizes MC38 cells *in vitro.* **A,** Evaluation of apoptosis and necrosis by Annexin V/Helix green dual staining assay after the 2Gy or 7Gy IR in the presence of 100 nmol/L, 1 µmol/L AZD7648 or DMSO. The experiments were carried out at least three times and the representative counter plot of 72 hours after IR were shown. The number in box represents % of total cells. **B,** Mean of three technical replicates and SD of Annexin V^+ Helix $green^-$ proportion at indicated time points were shown in graph. The experiments were carried out at least three times and the representative result is shown. Error bar = mean ± SD, two-way ANOVA, Tukey's multiple comparison test (*$P < 0.05$; ****, $P < 0.0001$; n.s., nonsignificant). **C,** Mean of three technical replicates and SD of Annexin V^+ Helix $green^+$ proportion at indicated time points were shown in graph. Error bar = mean ± SD, two-way ANOVA, Tukey's multiple comparison test (*, $P < 0.05$; ****, $P < 0.0001$; n.s., nonsignificant). **D,** Clonogenic survival of MC38 cells *in vitro* with indicated IR dose in the presence of 100 nmol/L, 1 µmol/L AZD7648 or DMSO. Each data point is the mean of three technical replicates and error bar represents SD. The experiments were carried out at least three times and the representative result is shown.

effects; most significant effects on both populations were observed at 72 hours after 7Gy IR (**Fig. 2A–C**). To investigate if the cell death induced by IR and AZD7648 includes caspase dependent apoptosis, the pan-caspase inhibitor, QVD, was added prior to treatment with IR. Both Annexin-V^+Helix $green^-$ and Annexin-V^+Helix $green^+$ populations induced by the prototypical apoptosis inducer staurosporine (STS) were significantly reduced in the presence of QVD at 24, 48, and 72 hours posttreatment (Supplementary Figs. S1A and S1B). QVD treatment reduced the Annexin-V^+Helix $green^-$ percentage at 48 and 72 hours after 2Gy plus 1 µmol/L AZD7648 or after 7Gy ± 100 nmol/L or 1 µmol/L AZD7648 (Supplementary Fig. S1A). The proportion of Annexin-V^+Helix $green^+$ was unchanged or even slightly increased in the presence of QVD after 48 and 72 hours after IR in combination with 1 µmol/L AZD7648 (Supplementary Fig. S1B).

To further investigate the ability of AZD7648 to radiosensitize MC38 cells, clonogenic survival assays were performed following IR and AZD7648 treatment. The plating efficiency of the unirradiated MC38 cells was approximately 25%, which was not affected by treatment with either 100 nmol/L or 1 µmol/L of AZD7648 (Supplementary Table S1). A dose-dependent radiosensitization effect of AZD7648 was observed. DEF_{37} was calculated to be 2.02 at 1 µmol/L and 1.07 at 100 nmol/L. (**Fig. 2D**; Supplementary Table S1).

AZD7648 combination with RT significantly improved tumor control in syngeneic models

Next, we tested the antitumor activity of the AZD7648 and RT combination in MC38, CT26, and B16-F10 syngeneic cell line tumors, implanted in immuno-competent mice (study schema outlined

in **Fig. 3A** and **D**; Supplementary Fig. S2A). As a monotherapy, 10Gy RT delivered in five daily fractions significantly improved tumor control but led to few curative responses in mice bearing either MC38 (0/12 mice; **Fig. 3B** and **C**) or CT26 tumors (2/12 mice; **Fig. 3E** and **F**). There was no RT monotherapy benefit on B16-F10 growth control (Supplementary Figs. S2B and S2C). Monotherapy with AZD7648 did not result in tumor growth inhibition in any of these tumor model studies. However, a combination of AZD7648 and RT significantly improved tumor control with 75% (9/12 mice) and 42% (5/12 mice) showing complete tumor regression in MC38 and CT26 models, respectively (**Fig. 3B**, **C**, **E**, and **F**), and significantly prolonged tumor control in the B16-F10 model (RT vs. RT + AZD7648: median survival 7 and 9.5 days, respectively, $P = 0.03$; Supplementary Fig. S2C). We observed temporary bodyweight loss of up to 20% in AZD7648 and RT groups in all models, which recovered rapidly 4 to 5 days after final dosing (Supplementary Fig. S3). Forty to 50% of mice in the AZD7648 + RT group, but not in the RT-only group, developed radiation-induced dermatitis approximately 2 weeks post RT, which also resolved. We then sought to determine whether RT dose fractionation may impact tumor control when combined with AZD7648 (33, 34). Mice received either 10Gy in five fractions or a single dose of 7Gy RT with or without AZD7648 administration. Tumor control with monotherapy RT delivered as 10Gy in five fractions was superior to that of a single dose of 7Gy. When AZD7648 was combined with either fractionated or a single dose of RT, both regimens resulted in complete tumor regressions in 8 of 9 mice (fractionated) and 5 of 9 mice (single dose). However, there was no statistically significant difference in survival of mice between these combination regimens (Supplementary Fig. S4).

Complete tumor regression following AZD7648 and irradiation is $CD8^+$ T-cell dependent

To investigate the immunologic contribution to the antitumor activity of combination therapy with RT and AZD7648, MC38 tumors were implanted into nude (athymic, T-cell deficient) mice. The growth rate of the vehicle-treated MC38 tumors was not significantly different when implanted in either wildtype or nude mice ($P < 0.10$; Supplementary Table S2). RT delayed tumor growth compared with the vehicle-only treated group in nude mice (Vehicle vs. RT: median survival, 10 and 12 days, respectively, $P = 0.004$), however the growth delay was shorter than was observed in the IR-treated immunocompetent mice (median survival differences between Vehicle and RT: nude = 2 days, C57BL/6 = 13 days). Importantly, the strong combinatorial effect of AZD7648 and RT observed in immunocompetent mice was lost in the nude mice, and no complete tumor regressions were observed (**Figs. 3B** and **C** and **4A** and **B**). Also, there was no statistical difference in tumor growth rate between RT and AZD7648 + RT combination groups in nude mice (RT vs. RT + AZD7648 growth rate: 0.147 ± 0.033 vs. 0.112 ± 0.050 $\log_{10}(cm^3)$/day, $P = 0.30$; Supplementary Table S2). These data strongly suggest that the antitumor immune response generated following the AZD7648 and RT combination contributes to the improved efficacy observed.

Building on the data in nude mice, we investigated how treatment with AZD7648 and RT modulated the frequency and phenotype of tumor-infiltrating NK and $CD8^+$ T cells. Pharmacodynamic profiling of TILs was undertaken using flow cytometry 7 days after initial RT dose (Supplementary Fig. S5A). RT increased the proportion of NK cells within both leukocyte (Vehicle vs. RT: $4.4 \pm 0.9\%$ vs. $6.9 \pm 3.4\%$, $P < 0.0001$) and live cell populations (Vehicle vs. RT: $2.7 \pm 0.7\%$ vs. $4.9 \pm 3.5\%$, $P < 0.0001$) and AZD7648 and RT further significantly increased this proportion within live cells (RT vs. RT + AZD7648: $4.9 \pm 3.5\%$ vs. $8.0 \pm 2.9\%$, $P = 0.04$), and increased trend within leukocytes (RT vs. RT + AZD7648: $6.9 \pm 3.4\%$ vs. $9.5 \pm 3.6\%$, $P = 0.07$; **Fig. 4C** and **D**). Treatments did not impact the percentage of $CD8^+$ T cells within total live cells (**Fig. 4F**). The percentage of $CD8^+$ T cells within the $CD45^+$ leukocyte population showed a modest increase in response to RT (Vehicle vs. RT: $3.8 \pm 1.8\%$ vs. $4.3 \pm 1.2\%$, $P = 0.06$) but this decreased in the combination-treated group (RT vs. RT + AZD7648: $4.3 \pm 1.2\%$ vs. $2.9 \pm 1.7\%$, $P = 0.006$; **Fig. 4G**). RT led to an increased percentage of Granzyme B (GzmB) expressing tumor-infiltrating NK cells, which was found to be further increased when combined with AZD7648 (RT vs. RT + AZD7648: $66.3 \pm 3.3\%$ vs. $82.1 \pm 7.9\%$, $P < 0.0001$; **Fig. 4E**). However, no change in the proportion of GzmB-positive $CD8^+$ T cells was observed (Fig. 4H). Interestingly, PD-1 expression on $CD8^+$ T cells was significantly increased following RT (Vehicle vs. RT: median fluorescent intensity (MFI), $3{,}936 \pm 706$ vs. $5{,}521 \pm 1{,}025$, $P = 0.0001$). In contrast, addition of AZD7648 to RT resulted in significantly decreased PD-1 expression (RT vs. RT + AZD7648: MFI $5{,}521 \pm 1{,}035$ vs. $2{,}867 \pm 613$, $P < 0.0001$; **Fig. 4I**). As PD-1 is expressed by both activated and exhausted T cells, and to distinguish those populations, cells were analyzed for expression of another exhaustion marker, Lag-3 (Supplementary Fig. S5B). Although there was a numerical increase in the proportion of PD-1^+Lag-3^+ "exhausted" $CD8^+$ T cells following RT alone, this was not statistically significant ($P = 0.06$). However, when mice received RT in combination with AZD7648 the proportion of PD-1^+Lag-3^+ $CD8^+$ T cells was significantly reduced when compared with either RT or vehicle-only groups (Vehicle vs. RT + AZD7648: $49.3 \pm 7.6\%$ vs. $26.1 \pm 8.2\%$, $P < 0.0001$; RT vs. RT + AZD7648: $58.3 \pm 6.3\%$ vs. $26.1 \pm 8.2\%$, $P < 0.0001$; Supplementary Fig. S5C). Interestingly, although both monotherapies led to a small but significant ($P = 0.001$) increase in the frequency of p15e specific T cells (p15e is an MHC-I restricted epitope of endogenous mouse retrovirus, and is reported to be an MC38 tumor antigen; ref. 35) within $CD8^+$ T cells, this was not further increased in mice that received RT combination with AZD7648 (Supplementary Fig. S5D).

To further define the relative contribution of $CD4^+$ T cells, $CD8^+$ T cells, and NK cells to tumor control following treatment with RT and AZD7648, we evaluated the effect of $CD4^+$ T cell, $CD8^+$ T cell, or NK cell depletion studies. Although the depletion of $CD4^+$ T cells and NK cells had no observable impact on tumor control, the depletion of $CD8^+$ T cells significantly reduced the efficacy of combined therapy with RT and AZD7648 (**Fig. 4J** and **K**; Supplementary Fig. S6). In the absence of $CD8^+$ T cells, tumor growth was accelerated both in vehicle and RT groups (Vehicle vs. Vehicle + αCD8: 0.149 ± 0.025 vs. 0.180 ± 0.012 $\log_{10}(cm^3)$/day, $P = 0.004$; RT vs. RT + αCD8: 0.083 ± 0.032 vs. 0.122 ± 0.025 $\log_{10}(cm^3)$/day, $P = 0.004$; Supplementary Fig. S7). The combination of RT and AZD7648 was found to improve tumor control when compared with RT alone (median survival: 38 days vs. 24 days, respectively, $P = 0.002$). However, in the absence of $CD8^+$ T cells, combination therapy did not lead to complete tumor regression in any mice (**Fig. 4J**). Collectively, these results indicate that AZD7648 and IR treatment induces $CD8^+$ T cell–dependent antitumor immune responses which contribute to tumor control.

Tumor control following combination of RT and AZD7648 is dependent on type I IFN

Accumulating evidence shows that type I IFNs are drivers of inflammation, support immune priming, and that this pathway is also important for the immunogenicity of radiotherapy (24–26, 28, 29, 36). We hypothesized that combination treatment of AZD7648 with RT would further upregulate type I IFN signaling. To

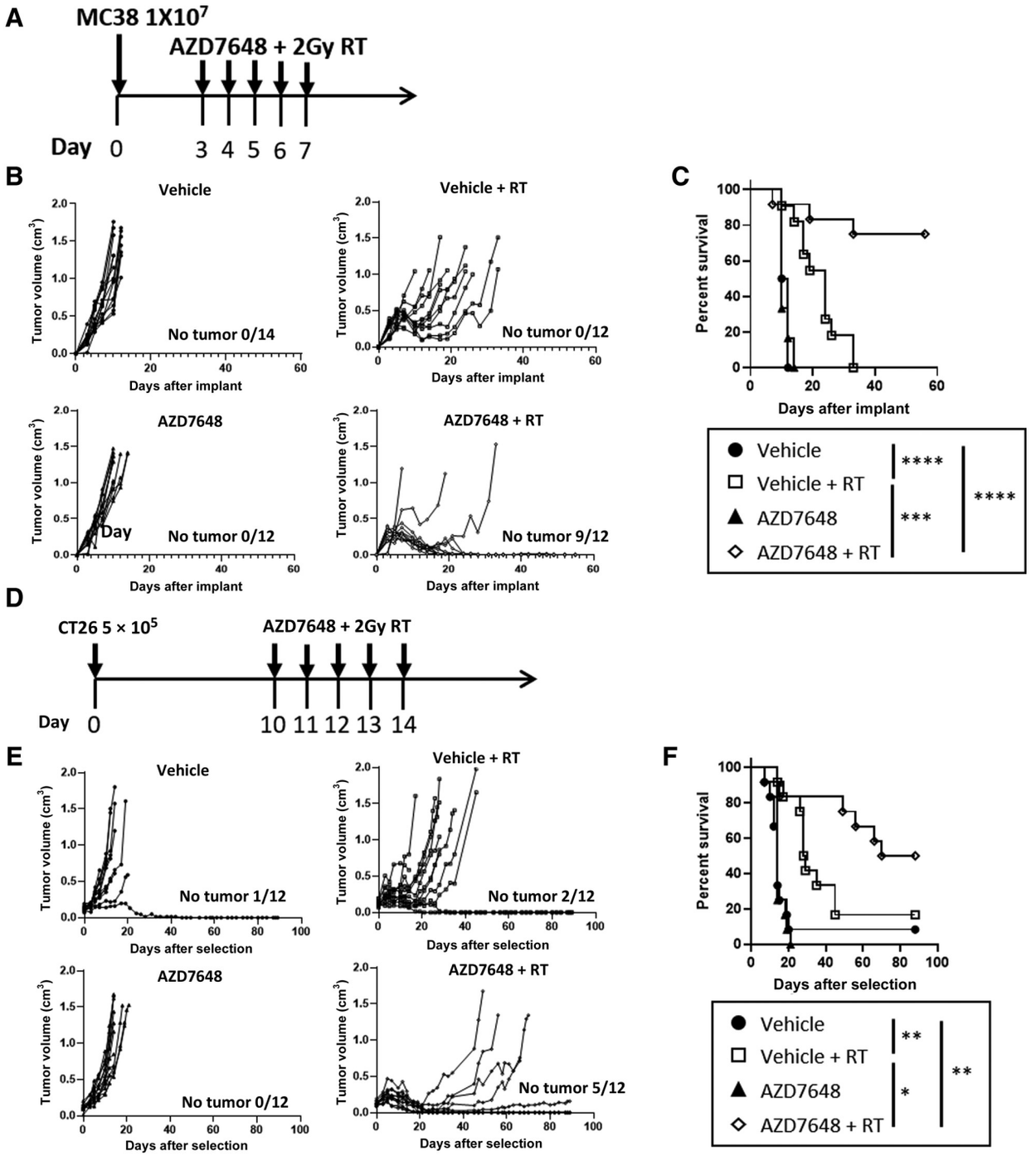

Figure 3.

AZD7648 and tumor-targeted RT controls tumor growth longer than each monotherapy in syngeneic mouse models. **A,** Dosing schedule to MC38-bearing C57BL/6 mice. Dosing started at day 3 post tumor implant and dosed every day till day 7. AZD7648 (75 mg/kg) was orally administered 1 to 2 hours before tumor-targeted RT (2Gy). **B,** Individual animal's tumor growth over time from implant day with the treatment of AZD7648 (75 mg/kg), 2Gyx5 RT, or the combination of both. **C,** Kaplan–Meier survival curve of C57BL/6 mice treated with AZD7648 (75 mg/kg), 2Gyx5 RT, or the combination of both from the data (**B**). Cut-off point is when tumor volume reached 1 cm^3 (log-rank test; ***, $P < 0.001$; ****, $P < 0.0001$). **D,** Dosing schedule to CT26-bearing Balb/c mice. Mice were dosed every day from day 10 post tumor implant until day 14. AZD7648 (75 mg/kg) was orally administered 1 to 2 hours before tumor-targeted RT (2Gy). **E,** Individual animal's CT26 tumor growth over time with the treatment of AZD7648 (75 mg/kg), 2Gyx5 RT, or the combination of AZD7648 plus RT. **F,** Kaplan–Meier survival curve of Balb/c mice in **E**. Cut-off point is when tumor volume reached 1.5 cm^3 or tumor erosion was observed (log-rank test; *, $P < 0.05$; **, $P < 0.01$).

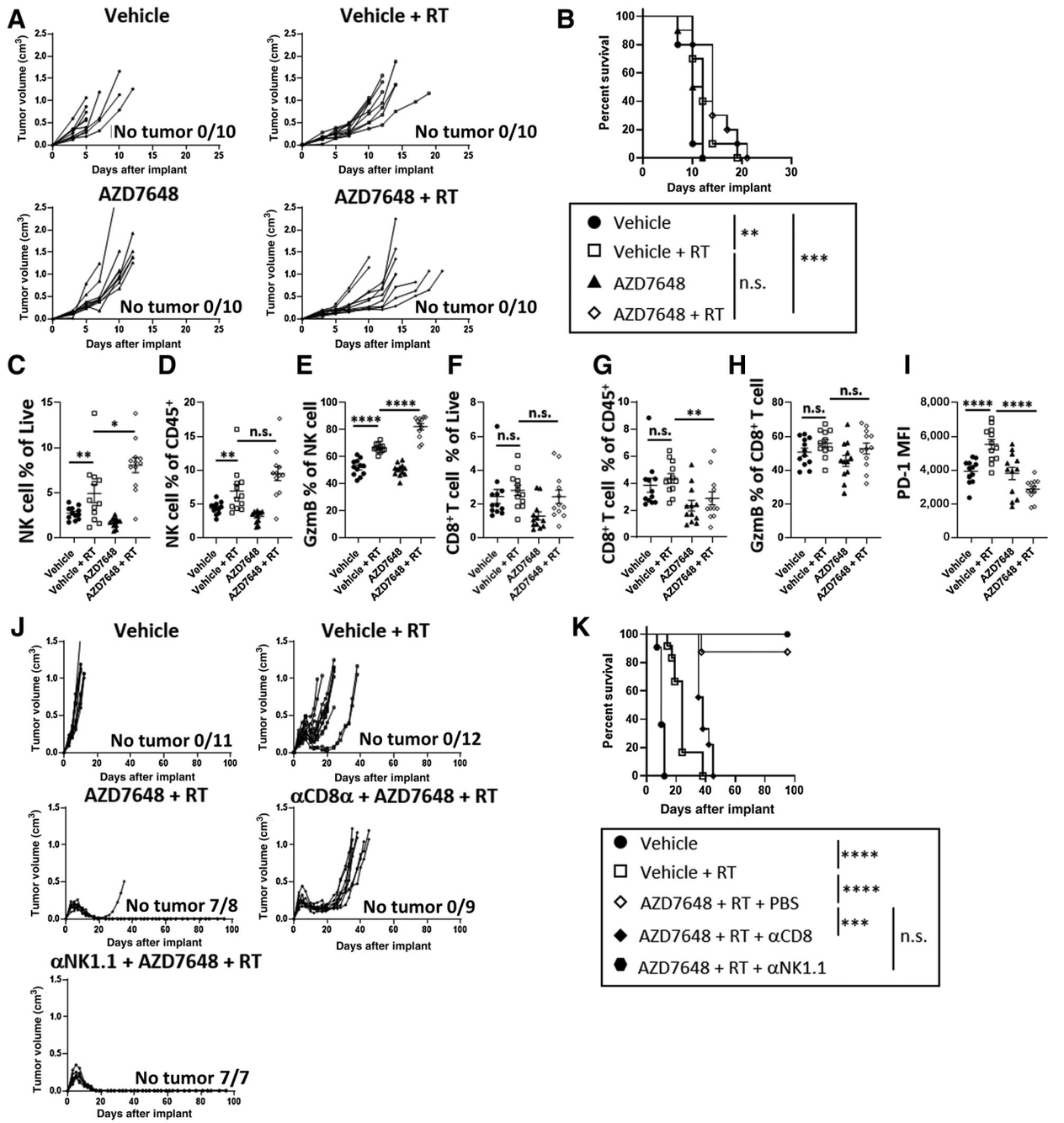

Figure 4.

CD8$^+$ T-cell dependent but NK-cell independent antitumor effect induced by AZD7648 plus tumor-targeted IR in MC38 syngeneic model. **A,** Individual animal's tumor growth over time with the treatment of AZD7648 (75 mg/kg), 2Gyx5 RT, or the combination of AZD7648 plus RT in athymic nude mice hosts. **B,** Kaplan–Meier survival curve of nude mice treated with AZD7648 (75 mg/kg), 2Gyx5 RT, or the combination of both from the data **A**. Cut-off point is when tumor volume reached 1 cm^3 or tumor erosion was observed (log-rank test, **, $P < 0.01$; ***, $P < 0.001$; n.s., nonsignificant). **C**–**I**, MC38 TILs were analyzed at day 7 after initial dosing by flow cytometry. NK-cell proportion of live cells (**C**) and CD45$^+$ cells (**D**), and GzmB$^+$ proportion of NK cells (**E**). CD8$^+$ T-cell proportion of live cells (**F**) and CD45$^+$ cells (**G**), GzmB$^+$ proportion of CD8$^+$ T cells (**H**), and PD-1 MFI of CD8$^+$ T cells. **I**, Experiment was repeated three times and representative result was shown in figure ($n = 12$, error bar = median ± SEM, for proportion data and β-regression, and for MFI data, one-way ANOVA; *, $P < 0.05$; **, $P < 0.01$; ***, $P < 0.001$; ****, $P < 0.0001$, n.s., nonsignificant). **J,** 10 mg/kg of anti-CD8α or anti-NK1.1 antibody were administered (days 2, 3, 10, 11, 18 and days 2, 3, 11, 25, respectively) interperitoneally in C57BL/6 mice and AZD7648 (75 mg/kg) orally administered plus tumor-targeted IR days 3 to 7. Individual animal's tumor growth over time was plotted. **K,** Kaplan–Meier survival curve of C57BL/6 mice from **J**. Cut-off point is when tumor volume reached 1 cm^3 or tumor erosion was observed (log-rank test; ***, $P < 0.001$; ***, $P < 0.001$; n.s., nonsignificant).

explore this, first *in vitro* cultured MC38 cells were treated with AZD7648 or vehicle, with and without IR, and expression of type I IFN and IFN stimulated genes (ISG) was analyzed. Consistent with previous reports (37, 38), IR treatment of MC38 cells induced the expression of type I IFN, *Ifnb1*, and the ISGs *Isg15, Mx1*, and *Cxcl10*, in a radiation dose-dependent manner (**Fig. 5A**). Treatment with AZD7648 plus IR further increased the expression of those genes as compared with IR only and this was more evident at 48 hours after treatment (**Fig. 5A**). To investigate whether an IFN autocrine loop also contributes to the expression of ISGs in MC38 cells treated with AZD7648 and IR, the receptor for type I IFN was blocked by mAb prior to IR treatment. Upregulation of *Cxcl10, Ifnb1, Isg15*, and *Mx1* by IR occurred in a dose-dependent manner and was further increased by addition of AZD7648. Gene induction occurred in the presence of anti-IFNαR1 antibody, although expression was reduced when compared with non-antibody–treated cells (Supplementary Fig. S8).

To evaluate the *in vivo* upregulation of type I IFN responsive genes following AZD7648 and RT monotherapy and combination treatments, gene expression in MC38 tumors was analyzed. At 7 days after the initial dose of RT, the ISGs *Mx1, Mx2, Isg20, Irf7, Ifit2/3, Isg20, Ddx4*, and *Rsad2* were all significantly elevated in tumors following combination of AZD7648 and RT, compared with tumors from vehicle-, AZD7648-, or RT monotherapy–treated mice (**Fig. 5B**).

As the AZD7648 and RT combination resulted in *in vitro* and *ex vivo* upregulation of ISGs expression, we tested whether type I IFN signaling is important for inhibition of MC38 tumor growth. Receptors for type I IFNs were blocked via the administration of an anti-IFNαR1 antibody prior to the initial treatment and maintained for 5 weeks. Tumor growth in both the vehicle and RT groups was accelerated by blocking of IFNαR1 (Vehicle vs. Vehicle + αIFNαR1: 0.149 ± 0.025 vs. 0.187 ± 0.008 $\log_{10}$ (cm^3)/day, $P = 0.002$; RT vs. RT + αIFNαR1: 0.083 ± 0.032 vs. 0.120 ± 0.037 $\log_{10}$ (cm^3)/day, $P = 0.03$; Supplementary Fig. S7). Although the combination of AZD7648 and RT plus IFNαR1 blocking antibody resulted in significantly longer tumor growth control compared with RT alone (median survival 41 and 20 days, respectively, $P < 0.0001$), tumor growth control was not durable, as tumors grew back in the majority of mice, with only 2 of 9 mice showing durable complete tumor regression (**Fig. 5C** and **D**). Together, these results demonstrate that combination of AZD7648 and RT enhances type I IFN production, which is required for maximal antitumor immune responses.

AZD7648 and RT generates long-term immunologic memory

Following our observations that MC38 and CT26 tumors treated with the combination of AZD7648 and RT achieved long-term tumor control, we hypothesized that immunologic memory developed against tumor antigens may suppress subsequent tumor challenge. To test this hypothesis, mice that had previously demonstrated complete tumor regression following AZD7648 and RT combination treatment were rechallenged by contralateral flank implantation of the same tumor cell line, whereas naive mice were similarly implanted as a control. Growth of tumors following a second implantation of MC38 cells was significantly delayed in mice that had previously achieved a complete tumor regression (**Fig. 6A–C**). As reported previously (39), in MC38 tumor model, increased dose of tumor cells in the rechallenge (Supplementary Fig. S9A) and increasing the time between complete initial tumor regression and rechallenge (Supplementary Fig. S9B) may have reduced the duration of second tumor control. B16-F10 tumor cells were also implanted into a cohort of mice that achieved a complete tumor regression following implantation of MC38 cells. Unexpectedly, the growth of the B16-F10 tumors was also slower in these mice, as compared with tumor-naïve mice (**Fig. 6A–C**). In contrast, rechallenge with CT26 cells did not result in tumor development during a monitoring period of ∼80 days in mice that had previously shown a complete CT26 tumor regression (**Fig. 6D** and **E**). These data demonstrated that AZD7648 plus RT established immunologic memory *in vivo* against tumor endogenous antigens.

Discussion

Here, we have demonstrated that the DNA-PK inhibitor, AZD7648, not only radiosensitizes syngeneic cell lines and increases tumor cell death, but can also modulate *in vivo* immune responses when combined with RT. The importance of the immune response for *in vivo* tumor growth control by the combination is supported by our observations that efficacy is reduced in the absence of either $CD8^+$ T cells or type I IFN signaling, and that the combination results in functional antitumor immunologic memory.

DNA-PK is activated early in the NHEJ DNA repair pathway in response to DNA DSB. DNA-PK inhibition, together with radiation or topoisomerase II inhibitors, has been shown to induce genome instability and accumulation of DNA lesions, which then ultimately leads to cell death (14–17). Drug targeting of NHEJ could be clinically attractive because NHEJ is active in all phases of the cell cycle, in contrast to agents only active during specific points in the cell cycle. Furthermore, targeting NHEJ could lead to further tumor death through synthetic lethality if the tumor is homologous-recombination pathway deficient as seen in ATM-deficient cells (14). In agreement with preceding studies (14), we have shown that AZD7648 radiosensitizes the syngeneic cell line, MC38, in a dose-dependent manner with $DEF_{37} = 2.02$ at 1 μmol/L AZD7648 (**Fig. 2D**). Surprisingly, despite the radiosensitization observed *in vitro* with AZD7648, we did not observe this to the same extent *in vivo* in the nude mouse model. We suggest that this is a consequence of factors such as hypoxia and tissue specific mitogenic/survival cues that may influence repopulation and therefore the intrinsic radiobiological effect (40, 41). DEF_{37} at 1 μmol/L of AZD7648 in MC38 cells was relatively modest compared with that observed for the human tumor cell lines, A549 and NCI-H1299 (DEF_{37} at 1 μmol/L AZD7648 = 5.1 and 7.4, respectively; ref. 14). Despite that, combination of AZD7648 and RT *in vivo* in the MC38 model resulted in 75% to 100% (across studies) of treated animals achieving complete tumor regression (**Figs. 3B**, **4J**, and **5C**; Supplementary Figs. S4A and S6A). This is comparable with the efficacy reported for this combination in NCI-H1299, and greater than previously reported for A549 *in vivo* (14). These data support the concept that additional mechanisms other than the direct cytoreductive effects of RT and AZD7648, such as antitumor immune responses, contribute to the long-lasting tumor control observed in this study across a range of syngeneic models.

It is now widely accepted that increasing the expression of type I IFN can promote antitumor immune responses by supporting the priming of adaptive immunity (24–26, 28, 29, 36). Our study showed that RT combined with DNA-PK inhibition elevated the expression of ISGs and that the expression of IFN in the tumor microenvironment was required for durable tumor growth control. Previous studies have reported that damaged nuclear DNA, free DNA, or cytosolic DNA, sensed either intrinsically by tumor cells or by DCs (which have engulfed dying tumor cells), can activate DNA sensing pathways, such as cGAS, ATM, and IFI16, leading to STING activation and type I IFN production (25, 26, 42–46). Activation of the cGAS–STING pathway has been reported to occur spontaneously in immunogenic tumors (25) and DDR-deficient/inhibited tumors (45, 46). Type I IFN

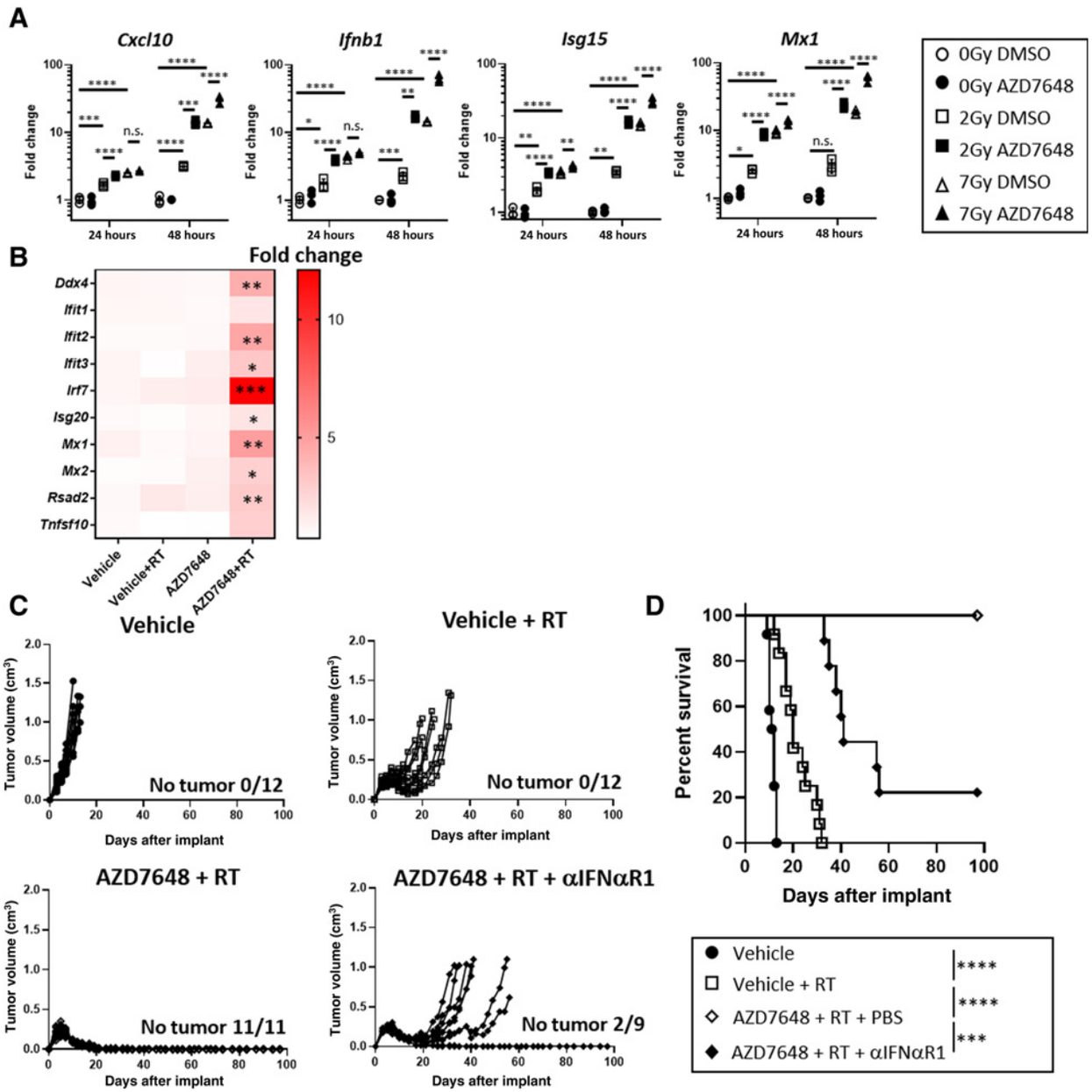

Figure 5.

Type I IFN signal upregulation following AZD7648 + IR treatment is key for tumor growth control. **A,** qPCR to measure gene expression of type I IFN responsive genes in MC38 treated with IR and AZD7648 (1 μmol/L). Fold change of gene of interest from the average expression level of 0Gy DMSO sample at each time point. Data represent mean and SD ($n = 3$). Experiment was repeated twice and representative result was shown in figure. One-way ANOVA, Tukey's multiple comparison test (*, $P < 0.05$; **, $P < 0.01$; ***, $P < 0.001$; ****, $P < 0.0001$; n.s., nonsignificant). **B,** Heat map of relative type I IFN responsive genes expression level in RNA isolated from MC38 tumor after the treatment of Vehicle, RT (2Gyx5), AZD7648 (75 mg/kg), or AZD7648 + RT at 7 days after initial dosing. Vehicle $n = 7$, Vehicle + RT $n = 8$, AZD7648 $n = 12$, AZD7648+RT $n = 7$. Fold changes from average gene expression level in each gene in vehicle-treated group were shown. Kruskal–Wallis test, Dunn's multiple comparison test (*, $P < 0.05$; **, $P < 0.01$; ***, $P < 0.001$). **C,** 5 mg/kg of anti-IFNαR1 antibody was administered via interperitoneal injection to C57BL/6 mice from day 2 after cell implant then administered three times per week for 5 weeks; AZD7648 (75 mg/kg) was orally administered 1 to 2 hours before the tumor-targeted RT (2Gy) days 3 to 7. Individual animal's tumor growth over the time was plotted. **D,** Kaplan–Meier survival curve of C57BL/6 mice from **C**. Cut-off point is when tumor volume reached 1 cm^3 or tumor erosion was observed (log-rank test; ***, $P < 0.001$; ***, $P < 0.001$).

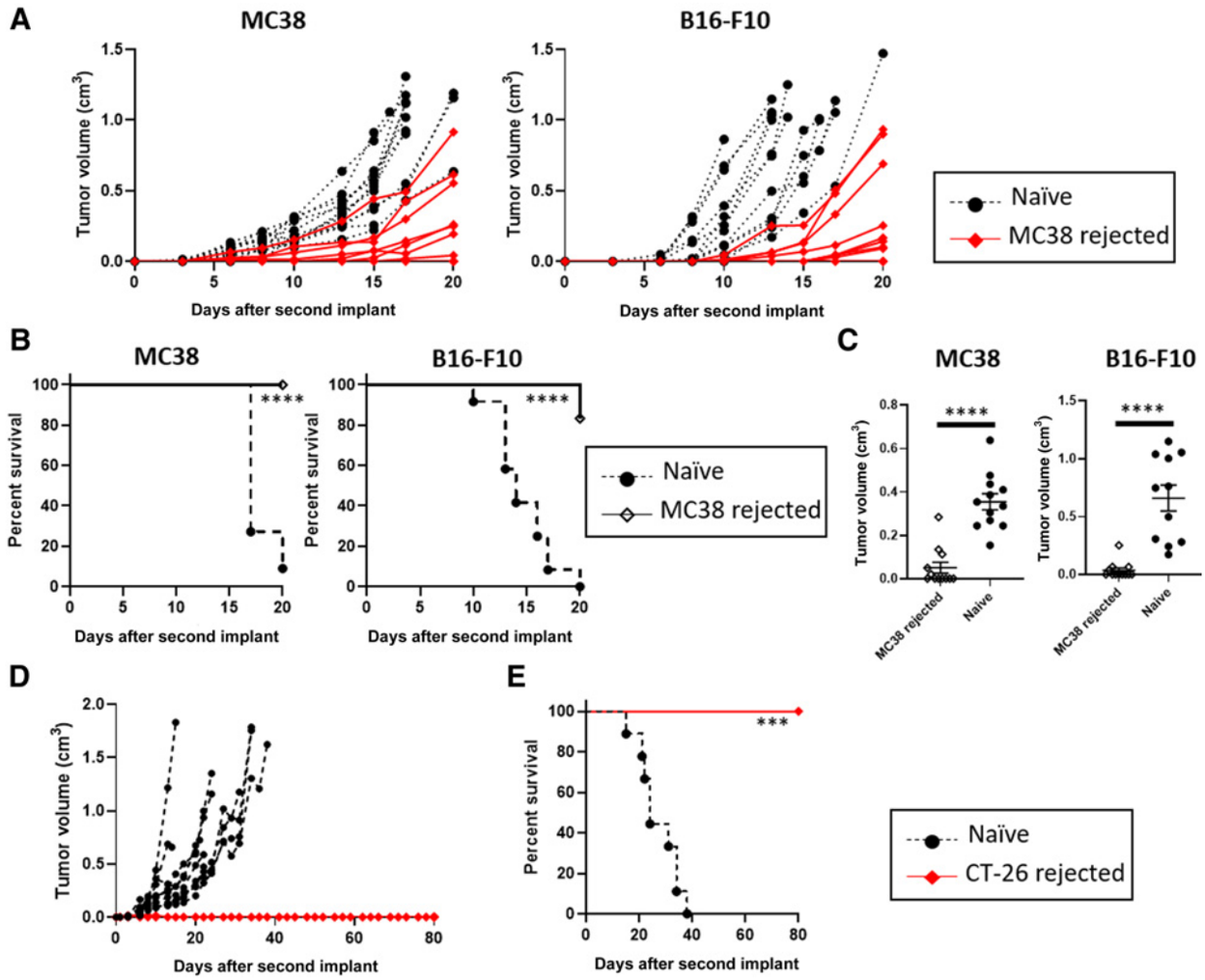

Figure 6.

AZD7648 and tumor-targeted IR promotes immunologic memory against tumor antigen. **A,** MC38 (5×10^5) or B16-F10 (1×10^5) cells were rechallenged 15 days after tumor complete regression. As a control, tumor was implanted to naïve C57BL/6 mice same time as rechallenged mice. Naïve mice $n = 12$, complete responder $n = 12$ for each cell line implant. **B,** Kaplan–Meier survival curves of rechallenged and naïve C57BL/6 mice from **A**. Cut-off point is when tumor reached 1 cm^3 or tumor erosion was observed (log-rank test; ****, $P < 0.0001$). **C,** Tumor volume of rechallenged tumor at day 13. Error bar represents mean and SE (Mann–Whitney test; ****, $P < 0.0001$). **D,** 5×10^5 CT26 were rechallenged approximately 60 days after tumor complete regression. Same lot and number of CT26 were implanted to naïve Balb/c mice at the same time to use as control. Naïve mice $n = 10$, complete responder $n = 5$. **E,** Kaplan–Meier survival curve of rechallenged and naïve Balb/c mice from **C**. Cut-off point is when tumor reached 1 cm^3 or tumor erosion was observed (log-rank test; ****, $P < 0.0001$).

expression can occur in response to treatment with DNA-damaging agents such as RT (24, 47), topoisomerase II inhibitors (48), and DDR inhibitors in DDR-deficient tumor cells by inducing synthetic lethality (42). Micronuclei can be formed as a result of chromosome instability, such as that observed with cell-cycle checkpoint failure following DNA damage (4, 44, 49), and these are also reported to stimulate the cGAS-STING-type I IFN axis following membrane rupture (44, 49). We have previously reported that combination of RT and AZD7648 induces formation of micronuclei in FaDu and FaDu $ATM^{-/-}$ cells (14). In another study, however, treatment with DNA-PK inhibitors was reported to suppress the formation of micronuclei and subsequent activation of inflammatory signaling such as type I IFN (marked by phosphorylation of STAT-1) following IR due to the triggering of the G_2–M checkpoint (44). Stimulation of the cGAS-STING-type I IFN pathway by intracellular DNA has been reported to lead to the activation of receptor interacting protein kinases 3 (RIPK3) and immunogenic necroptosis (50). Therefore, this might partly contribute to the significant increase of the Annexin V^+Helix $green^+$ population *in vitro* following combination treatment with AZD7648 plus IR (**Fig. 2A** and **C**). Interestingly, both caspase dependent and independent cell death was induced by AZD7648 and IR (Supplementary Fig. S1) in agreement with a report that several types of cell death (apoptosis, necrosis, necroptosis) are induced following IR (51). Blockade of type I IFN activity *in vivo* with an anti-IFNαR1 antibody attenuated complete tumor regression. This demonstrates that type I IFN induction in response to the combination of AZD7648 and RT is

important for antitumor activity. However, the role of type I IFN can be paradoxical as previous studies have also reported that the expression of ISGs are associated with resistance to RT or chemotherapy (52, 53). This might be explained by the differential role of type I IFN in immune cells (i.e., immune activation, antitumor) and some neoplastic cells (i.e., resistance to cytotoxicity, protumor; ref. 37). Moreover, data suggest that although acute activation of type I IFN can promote antitumor activity, chronic type I IFN may lead to tumor resistance from immune effector function (54, 55). It would be interesting to explore how the duration of type I IFN signaling would influence efficacy of the AZD7648 and RT combination.

Previous studies have reported that DDR inhibitor treatment of DDR deficient ($p53^{-/-}$Brca-$1^{-/-}$ c-Myc transformed ovarian tumor) or proficient (Hepa 1–6 liver, oncogene transformed TC-1 lung, CT26 colorectal) tumors, either alone or in combination with RT, resulted in increased cytotoxic cells and DC infiltration and activation (42, 47, 56, 57). One of the mechanisms responsible is the multi-immunomodulatory activity of type I IFN; induction of chemo attractants such as Cxcl10 in the tumor microenvironment upregulates the costimulatory molecules in antigen presenting cells leading to local immune priming and cell proliferation (24, 28, 29). In this study, we observed the significant up-regulation of *Cxcl10* (**Fig. 5A**) and increased frequency of total and GzmB-expressing NK cells and reduced infiltration of exhausted $CD8^+$ T cells by the treatment of RT and AZD7648 (**Fig. 4C–E** and **I**; Supplementary **Fig. S5C**). The importance of those $CD8^+$ T cells in complete tumor regression was demonstrated by *in vivo* antibody-mediated depletion (**Fig. 4J** and **K**).

Radiation dose fractionation has been shown to influence the generation and magnitude of the antitumor immune response with data supporting activity of either single ablative doses, hypofractionated RT, or fractionated RT in different preclinical models (33, 34, 58, 59). Indeed, multiple mechanisms may influence the relative immunogenicity of the different RT dose and fractionation schedules including intrinsic radiosensitivity, level of immune effector cell infiltrate, and the balance of these with suppressive features of the tumor microenvironment. In our model, 10Gy in five fractions and a single dose of 7Gy demonstrated similar antitumor efficacy in combination with AZD7648 (Supplementary Fig. S4). Although beyond the scope of the present study, it would be interesting to further explore how RT dose fractionation (including hypofractionated RT) would impact the antitumor response across a range of models in combination with AZD7648.

The combination of AZD7648 plus IR induced formation of immunologic memory, as demonstrated by the delayed or complete protection from tumor growth exhibited in tumor-free survivors rechallenged with tumor cells. Interestingly, in our model, mice that underwent complete responses against MC38 tumors following AZD7648 plus RT treatment were also protected from B16-F10 tumor challenge (**Fig. 6A–C**). This observation may be due to the establishment of immunologic memory to shared tumor antigens between MC38 and B16-F10. The endogenous ecotropic murine retroviral envelope protein, p15e, has been suggested as a candidate shared antigen (35), however increased infiltration by p15e-specific $CD8^+$ T cells was not observed following the treatment of RT and AZD7648 (Supplementary Fig. S5D). Common mutations between MC38 and B16-F10 could also contribute to the delayed growth of both tumors, however, no common mutations have been identified in MC38 and B16-F10 (60). Therefore, other, undefined common antigens could also contribute to the specificity of memory T cells including other immunogenic peptides reported to be sufficient to establish memory responses in the absence of p15e (61).

In summary, we have shown that DNA-PK inhibition in combination with RT is highly effective in eliminating tumor growth in syngeneic models. Moreover, these responses induce immunologic memory. These effects were mediated, at least in part, by upregulation of type I IFN responses. Our findings provide additional supporting evidence for the rationale of targeting components of the DNA damage response combined with RT to control tumors through immunologic mechanisms, in addition to direct antitumor effects (14). The potential to elicit immunologic memory provides hope that this combination may have curative potential in early disease settings, provided an acceptable balance of tolerability and efficacy can be achieved.

Authors' Disclosures

K. Nakamura reports personal fees and other support from AstraZeneca during the conduct of the study, as well as personal fees and other support from AstraZeneca outside the submitted work. P.M. Farrington reports personal fees and other support from AstraZeneca during the conduct of the study, as well as personal fees and other support from AstraZeneca outside the submitted work. A. Ramos-Montoya reports personal fees from AstraZeneca during the conduct of the study, as well as personal fees from AstraZeneca outside the submitted work. S.J. Bickerton reports personal fees from AstraZeneca during the conduct of the study, as well as personal fees from AstraZeneca outside the submitted work. G.D. Hughes reports personal fees from AstraZeneca during the conduct of the study. B.R. Davies reports personal fees from AstraZeneca during the conduct of the study. S.J. Dovedi reports personal fees and other support from AstraZeneca during the conduct of the study, as well as personal fees and other support from AstraZeneca outside the submitted work. V. Valge-Archer reports other support from AstraZeneca during the conduct of the study, as well as other support from AstraZeneca outside the submitted work. No disclosures were reported by the other authors.

Authors' Contributions

K. Nakamura: Conceptualization, formal analysis, validation, investigation, visualization, methodology, writing–original draft, writing–review and editing. **A. Karmokar:** Investigation, methodology. **P.M. Farrington:** Investigation, methodology. **N.H. James:** Investigation. **A. Ramos-Montoya:** Methodology, project administration. **S.J. Bickerton:** Investigation. **G.D. Hughes:** Methodology, project administration. **T.M. Illidge:** Resources, supervision, writing–original draft. **E.B. Cadogan:** Conceptualization, supervision, project administration. **B.R. Davies:** Conceptualization, supervision, funding acquisition, writing–original draft, project administration, writing–review and editing. **S.J. Dovedi:** Conceptualization, supervision, funding acquisition, writing–original draft, project administration, writing–review and editing. **V. Valge-Archer:** Conceptualization, supervision, funding acquisition, writing–original draft, project administration, writing–review and editing.

Acknowledgments

We thank Mr. Jonathan Greenall, Dr. Chiranjeevi Sandi, and staff from Animal Sciences and Technologies, AstraZeneca Alderley Park, for expert animal husbandry and procedure support, and Drs. Bairu Zhang, Benjamin Phillips, and Natasha Karp for statistical advice. We thank Cancer Research UK Manchester Institute staff Mr. Jeff Barry, Ms. Antonia Banyard, Mr. Michele Fresneda Alarcon, and Ms. Yosra Elagili for technical assistance with flow cytometry, and Dr. Kang Zhang, Dr. Swati Pendharkar, and Mr. Steven Bagley for technical support with the *in vitro* irradiation studies. Kyoko Nakamura was funded through the AstraZeneca postdoctoral program.

The costs of publication of this article were defrayed in part by the payment of page charges. This article must therefore be hereby marked *advertisement* in accordance with 18 U.S.C. Section 1734 solely to indicate this fact.

Received September 18, 2020; revised March 12, 2021; accepted May 14, 2021; published first May 19, 2021.

References

1. Martin OA, Martin RF. Cancer radiotherapy: understanding the price of tumor eradication. Front Cell Dev Biol 2020;8:261.
2. Baskar R, Dai J, Wenlong N, Yeo R, Yeoh KW. Biological response of cancer cells to radiation treatment. Front Mol Biosci 2014;1:24.
3. Pilie PG, Tang C, Mills GB, Yap TA. State-of-the-art strategies for targeting the DNA damage response in cancer. Nat Rev Clin Oncol 2019;16:81–104.
4. Dillon MT, Barker HE, Pedersen M, Hafsi H, Bhide SA, Newbold KL, et al. Radiosensitization by the ATR inhibitor AZD6738 through generation of acentric micronuclei. Mol Cancer Ther 2017;16:25–34.
5. Fokas E, Prevo R, Pollard JR, Reaper PM, Charlton PA, Cornelissen B, et al. Targeting ATR in vivo using the novel inhibitor VE-822 results in selective sensitization of pancreatic tumors to radiation. Cell Death Dis 2012;3:e441.
6. Wengner AM, Siemeister G, Lucking U, Lefranc J, Wortmann L, Lienau P, et al. The novel ATR inhibitor BAY 1895344 is efficacious as monotherapy and combined with DNA damage-inducing or repair-compromising therapies in preclinical cancer models. Mol Cancer Ther 2020;19:26–38.
7. Dungey FA, Loser DA, Chalmers AJ. Replication-dependent radiosensitization of human glioma cells by inhibition of poly(ADP-ribose) polymerase: mechanisms and therapeutic potential. Int J Radiat Oncol Biol Phys 2008;72:1188–97.
8. Noel G, Godon C, Fernet M, Giocanti N, Megnin-Chanet F, Favaudon V. Radiosensitization by the poly(ADP-ribose) polymerase inhibitor 4-amino-1,8-naphthalimide is specific of the S phase of the cell cycle and involves arrest of DNA synthesis. Mol Cancer Ther 2006;5:564–74.
9. Zhao W, Hu H, Mo Q, Guan Y, Li Y, Du Y, et al. Function and mechanism of combined PARP-1 and BRCA genes in regulating the radiosensitivity of breast cancer cells. Int J Clin Exp Pathol 2019;12:3915–20.
10. Durant ST, Zheng L, Wang Y, Chen K, Zhang L, Zhang T, et al. The brain-penetrant clinical ATM inhibitor AZD1390 radiosensitizes and improves survival of preclinical brain tumor models. Sci Adv 2018;4:eaat1719.
11. Hickson I, Zhao Y, Richardson CJ, Green SJ, Martin NM, Orr AI, et al. Identification and characterization of a novel and specific inhibitor of the ataxia-telangiectasia mutated kinase ATM. Cancer Res 2004;64:9152–9.
12. Rainey MD, Charlton ME, Stanton RV, Kastan MB. Transient inhibition of ATM kinase is sufficient to enhance cellular sensitivity to ionizing radiation. Cancer Res 2008;68:7466–74.
13. Riches LC, Trinidad AG, Hughes G, Jones GN, Hughes AM, Thomason AG, et al. Pharmacology of the ATM inhibitor AZD0156: potentiation of irradiation and olaparib responses preclinically. Mol Cancer Ther 2020;19:13–25.
14. Fok JHL, Ramos-Montoya A, Vazquez-Chantada M, Wijnhoven PWG, Follia V, James N, et al. AZD7648 is a potent and selective DNA-PK inhibitor that enhances radiation, chemotherapy and olaparib activity. Nat Commun 2019;10:5065.
15. Timme CR, Rath BH, O'Neill JW, Camphausen K, Tofilon PJ. The DNA-PK inhibitor VX-984 enhances the radiosensitivity of glioblastoma cells grown in vitro and as orthotopic xenografts. Mol Cancer Ther 2018;17:1207–16.
16. Willoughby CE, Jiang Y, Thomas HD, Willmore E, Kyle S, Wittner A, et al. Selective DNA-PKcs inhibition extends the therapeutic index of localized radiotherapy and chemotherapy. J Clin Invest 2020;130:258–71.
17. Zenke FT, Zimmermann A, Sirrenberg C, Dahmen H, Kirkin V, Pehl U, et al. Pharmacologic inhibitor of DNA-PK, M3814, potentiates radiotherapy and regresses human tumors in mouse models. Mol Cancer Ther 2020;19:1091–101.
18. Honeychurch J, Illidge TM. The influence of radiation in the context of developing combination immunotherapies in cancer. Ther Adv Vaccines Immunother 2017;5:115–22.
19. Rodriguez-Ruiz ME, Vanpouille-Box C, Melero I, Formenti SC, Demaria S. Immunological mechanisms responsible for radiation-induced abscopal effect. Trends Immunol 2018;39:644–55.
20. Formenti SC, Rudqvist NP, Golden E, Cooper B, Wennerberg E, Lhuillier C, et al. Radiotherapy induces responses of lung cancer to CTLA-4 blockade. Nat Med 2018;24:1845–51.
21. Reits EA, Hodge JW, Herberts CA, Groothuis TA, Chakraborty M, Wansley EK, et al. Radiation modulates the peptide repertoire, enhances MHC class I expression, and induces successful antitumor immunotherapy. J Exp Med 2006;203:1259–71.
22. Ghiringhelli F, Apetoh L, Tesniere A, Aymeric L, Ma Y, Ortiz C, et al. Activation of the NLRP3 inflammasome in dendritic cells induces IL-1beta-dependent adaptive immunity against tumors. Nat Med 2009;15:1170–8.
23. Apetoh L, Ghiringhelli F, Tesniere A, Obeid M, Ortiz C, Criollo A, et al. Toll-like receptor 4-dependent contribution of the immune system to anticancer chemotherapy and radiotherapy. Nat Med 2007;13:1050–9.
24. Deng L, Liang H, Xu M, Yang X, Burnette B, Arina A, et al. STING-dependent cytosolic DNA sensing promotes radiation-induced type I interferon-dependent antitumor immunity in immunogenic tumors. Immunity 2014;41:843–52.
25. Woo SR, Fuertes MB, Corrales L, Spranger S, Furdyna MJ, Leung MY, et al. STING-dependent cytosolic DNA sensing mediates innate immune recognition of immunogenic tumors. Immunity 2014;41:830–42.
26. Han C, Liu Z, Zhang Y, Shen A, Dong C, Zhang A, et al. Tumor cells suppress radiation-induced immunity by hijacking caspase 9 signaling. Nat Immunol 2020;21:546–54.
27. Kang TH, Mao CP, Kim YS, Kim TW, Yang A, Lam B, et al. TLR9 acts as a sensor for tumor-released DNA to modulate anti-tumor immunity after chemotherapy. J Immunother Cancer 2019;7:260.
28. Burnette BC, Liang H, Lee Y, Chlewicki L, Khodarev NN, Weichselbaum RR, et al. The efficacy of radiotherapy relies upon induction of type i interferon-dependent innate and adaptive immunity. Cancer Res 2011;71:2488–96.
29. Lim JY, Gerber SA, Murphy SP, Lord EM. Type I interferons induced by radiation therapy mediate recruitment and effector function of CD8(+) T cells. Cancer Immunol Immunother 2014;63:259–71.
30. Bjorkman A, Du L, Felgentreff K, Rosner C, Pankaj Kamdar R, Kokaraki G, et al. DNA-PKcs is involved in IG class switch recombination in human B cells. J Immunol 2015;195:5608–15.
31. Ma Y, Pannicke U, Schwarz K, Lieber MR. Hairpin opening and overhang processing by an Artemis/DNA-dependent protein kinase complex in nonhomologous end joining and V(D)J recombination. Cell 2002;108:781–94.
32. Goldberg FW, Finlay MRV, Ting AKT, Beattie D, Lamont GM, Fallan C, et al. The discovery of 7-methyl-2-[(7-methyl[1,2,4]triazolo[1,5-a]pyridin-6-yl) amino]-9-(tetrahydro-2H-p yran-4-yl)-7,9-dihydro-8H-purin-8-one (AZD7648), a potent and selective DNA-dependent protein kinase (DNA-PK) inhibitor. J Med Chem 2020;63:3461–71.
33. Dovedi SJ, Cheadle EJ, Popple AL, Poon E, Morrow M, Stewart R, et al. Fractionated radiation therapy stimulates antitumor immunity mediated by both resident and infiltrating polyclonal T-cell populations when combined with PD-1 blockade. Clin Cancer Res 2017;23:5514–26.
34. Vanpouille-Box C, Alard A, Aryankalayil MJ, Sarfraz Y, Diamond JM, Schneider RJ, et al. DNA exonuclease Trex1 regulates radiotherapy-induced tumour immunogenicity. Nat Commun 2017;8:15618.
35. Yang JC, Perry-Lalley D. The envelope protein of an endogenous murine retrovirus is a tumor-associated T-cell antigen for multiple murine tumors. J Immunother 2000;23:177–83.
36. Fuertes MB, Kacha AK, Kline J, Woo SR, Kranz DM, Murphy KM, et al. Host type I IFN signals are required for antitumor CD8+ T cell responses through CD8 {alpha}+ dendritic cells. J Exp Med 2011;208:2005–16.
37. Chen J, Cao Y, Markelc B, Kaeppler J, Vermeer JA, Muschel RJ. Type I IFN protects cancer cells from CD8+ T cell-mediated cytotoxicity after radiation. J Clin Invest 2019;129:4224–38.
38. Jones KI, Tiersma J, Yuzhalin AE, Gordon-Weeks AN, Buzzelli J, Im JH, et al. Radiation combined with macrophage depletion promotes adaptive immunity and potentiates checkpoint blockade. EMBO Mol Med 2018;10:e9342.
39. Zaharoff DA, Hance KW, Rogers CJ, Schlom J, Greiner JW. Intratumoral immunotherapy of established solid tumors with chitosan/IL-12. J Immunother 2010;33:697–705.
40. Ma NY, Tinganelli W, Maier A, Durante M, Kraft-Weyrather W. Influence of chronic hypoxia and radiation quality on cell survival. J Radiat Res 2013;54:i13–22.
41. Kamochi N, Nakashima M, Aoki S, Uchihashi K, Sugihara H, Toda S, et al. Irradiated fibroblast-induced bystander effects on invasive growth of squamous cell carcinoma under cancer-stromal cell interaction. Cancer Sci 2008;99:2417–27.
42. Ding L, Kim HJ, Wang Q, Kearns M, Jiang T, Ohlson CE, et al. PARP inhibition elicits STING-dependent antitumor immunity in Brca1-deficient ovarian cancer. Cell Rep 2018;25:2972–80.
43. Dunphy G, Flannery SM, Almine JF, Connolly DJ, Paulus C, Jonsson KL, et al. Non-canonical activation of the DNA sensing adaptor STING by ATM and IFI16 mediates NF-kappaB signaling after nuclear DNA damage. Mol Cell 2018;71:745–60.
44. Harding SM, Benci JL, Irianto J, Discher DE, Minn AJ, Greenberg RA. Mitotic progression following DNA damage enables pattern recognition within micronuclei. Nature 2017;548:466–70.

45. Hartlova A, Erttmann SF, Raffi FA, Schmalz AM, Resch U, Anugula S, et al. DNA damage primes the type I interferon system via the cytosolic DNA sensor STING to promote anti-microbial innate immunity. Immunity 2015;42:332–43.
46. Shen J, Zhao W, Ju Z, Wang L, Peng Y, Labrie M, et al. PARPi triggers the STING-dependent immune response and enhances the therapeutic efficacy of immune checkpoint blockade independent of BRCAness. Cancer Res 2019; 79:311–9.
47. Sheng H, Huang Y, Xiao Y, Zhu Z, Shen M, Zhou P, et al. ATR inhibitor AZD6738 enhances the antitumor activity of radiotherapy and immune checkpoint inhibitors by potentiating the tumor immune microenvironment in hepatocellular carcinoma. J Immunother Cancer 2020;8:e000340.
48. Wang Z, Chen J, Hu J, Zhang H, Xu F, He W, et al. cGAS/STING axis mediates a topoisomerase II inhibitor-induced tumor immunogenicity. J Clin Invest 2019; 129:4850–62.
49. Mackenzie KJ, Carroll P, Martin CA, Murina O, Fluteau A, Simpson DJ, et al. cGAS surveillance of micronuclei links genome instability to innate immunity. Nature 2017;548:461–5.
50. Brault M, Olsen TM, Martinez J, Stetson DB, Oberst A. Intracellular nucleic acid sensing triggers necroptosis through synergistic type I IFN and TNF signaling. J Immunol 2018;200:2748–56.
51. Adjemian S, Oltean T, Martens S, Wiernicki B, Goossens V, Vanden Berghe T, et al. Ionizing radiation results in a mixture of cellular outcomes including mitotic catastrophe, senescence, methuosis, and iron-dependent cell death. Cell Death Dis 2020;11:1003.
52. Weichselbaum RR, Ishwaran H, Yoon T, Nuyten DS, Baker SW, Khodarev N, et al. An interferon-related gene signature for DNA damage resistance is a predictive marker for chemotherapy and radiation for breast cancer. Proc Natl Acad Sci U S A 2008;105:18490–5.
53. Post AEM, Smid M, Nagelkerke A, Martens JWM, Bussink J, Sweep F, et al. Interferon-stimulated genes are involved in cross-resistance to radiotherapy in tamoxifen-resistant breast cancer. Clin Cancer Res 2018;24:3397–408.
54. Benci JL, Xu B, Qiu Y, Wu TJ, Dada H, Twyman-Saint Victor C, et al. Tumor interferon signaling regulates a multigenic resistance program to immune checkpoint blockade. Cell 2016;167:1540–54.
55. Khodarev NN, Minn AJ, Efimova EV, Darga TE, Labay E, Beckett M, et al. Signal transducer and activator of transcription 1 regulates both cytotoxic and prosurvival functions in tumor cells. Cancer Res 2007;67:9214–20.
56. Dillon MT, Bergerhoff KF, Pedersen M, Whittock H, Crespo-Rodriguez E, Patin EC, et al. ATR inhibition potentiates the radiation-induced inflammatory tumor microenvironment. Clin Cancer Res 2019;25:3392–403.
57. Vendetti FP, Karukonda P, Clump DA, Teo T, Lalonde R, Nugent K, et al. ATR kinase inhibitor AZD6738 potentiates CD8+ T cell-dependent antitumor activity following radiation. J Clin Invest 2018;128:3926–40.
58. Filatenkov A, Baker J, Mueller AM, Kenkel J, Ahn GO, Dutt S, et al. Ablative tumor radiation can change the tumor immune cell microenvironment to induce durable complete remissions. Clin Cancer Res 2015;21:3727–39.
59. Lugade AA, Moran JP, Gerber SA, Rose RC, Frelinger JG, Lord EM. Local radiation therapy of B16 melanoma tumors increases the generation of tumor antigen-specific effector cells that traffic to the tumor. J Immunol 2005;174: 7516–23.
60. Zhong W, Myers JS, Wang F, Wang K, Lucas J, Rosfjord E, et al. Comparison of the molecular and cellular phenotypes of common mouse syngeneic models with human tumors. BMC Genomics 2020;21:2.
61. Ye X, Waite JC, Dhanik A, Gupta N, Zhong M, Adler C, et al. Endogenous retroviral proteins provide an immunodominant but not requisite antigen in a murine immunotherapy tumor model. Oncoimmunology 2020;9:1758602.